Catalytic Activity and Mechanistic Investigations of the Nitrido Molybdenum Complex [(PPP)Mo(≠N)(I)] in the Electrochemical Reduction of N 2

Théo Personeni, Barbara Rialland, Idir Benaissa, Soukaina Bennaamane, Lhoussain Khrouz, Andrea Mulas, Marie Fustier-Boutignon, Eric Clot, Nicolas Mézailles, Christophe Bucher

Catalytic activity and mechanistic investigations of the nitrido molybdenum complex [(PPP)Mo(≡N)(I)] in the electrochemical reduction of N_2

Théo Personeni [ab], Barbara Rialland [b], Idir Benaissa [b], Soukaina Bennaamane [b], Lhoussain Khrouz [a], Andrea Mulas [b], Marie Fustier-Boutignon [b], Eric Clot [b], Nicolas Mézailles [b], Christophe Bucher [a]**

[a]CNRS, ENS de Lyon, LCH, UMR 5182, 69342 Lyon cedex 07, France

[b]Laboratoire Hétérochimie Fondamentale et appliquée, Université Paul Sabatier, CNRS, 31062 Toulouse Cedex, France

[c]ICGM, Univ. Montpellier, CNRS, ENSCM, 1919 route de Mende 34293 Montpellier Cedex 5, France

Email : nicolas.mezailles1@univ-tlse3.fr; christophe.bucher@ens-lyon.fr

Abstract: In the context of environmental concern, waste reduction and energy saving measures, much efforts have recently focused on strategies allowing to efficiently transform N_2 into valuable NR_3 products. We report here the first electrocatalytic transformation of chloroboranes into aminoboranes using a (triphosphine)Mo-nitrido complex. Based on extensive electrochemical and spectroscopic characterizations, reaction intermediates are identified and a catalytic cycle is proposed, highlighting the crucial role of both solvent and electrolyte

Introduction

The Haber-Bosch process stands as one of the most important chemical transformations to mankind. It allows the synthesis of ca 200 million tons/year of NH_3 from N_2 and H_2 using heterogeneous catalyst

submitted to drastic conditions.[1] This key industrial process is not only important, it is also highly energy consuming due to its harsh conditions, as it requires ca 1-2 % of the world annual energy production, and generates ca 1.5 % of the global emissions due to the use of fossil fuels.[2,3] Although making fertilizers to feed the population is a sound investment of the energy production, in the current context of global warming, the development of alternative approaches to decrease the environmental impact of this reaction is of major importance.[2–4] Much efforts have focused over the past decades on strategies involving use of homogeneous molecular catalysts capable of transforming N_2 into valuable products. Major obstacles were encountered in pursuing these ambitious goals, including the low affinity of N_2 for metal ions and the low reactivity of most nitrogen-metal bonds. This explains the very limited number of catalytic processes discovered to date to successfully transform N_2 into NH_3, $N(SiMe_3)_3$ or $N(BCy_2)_3$.[2,5–15] Previous works have established that these issues stem largely from difficulties in controlling the stability of key intermediates involved in the multi-electron reduction of N_2.[16] Electrochemically-driven strategies have recently emerged as particularly promising for activating the catalytic properties of metal complexes and achieving a mild and selective reduction of N_2 into NH_3. Surprisingly, since the pioneering work of Pickett published in 1985, this approach has remained very little explored.[16–19] Still, electrochemical methods have proved useful to study the H^+-coupled electron transfer processes involved in the catalytic reduction of N_2 by the molybdenum complex $(HIPTN_3N)Mo$ or to split N_2 and generate nitride intermediates from $[ReCl_2(PNP)]$ or $(PPP)MoX_3$ (X = I, Br).[20–26] In 2016, Peters and coworkers demonstrated that N_2 can be converted to NH_3 by electrochemical reduction of a Fe-N_2 complex incorporating a "BP_3"-type ligand (~ 4.0 eq. per Fe, 28 % FE).[27] The few examples reported to date also suffer from selectivity issues due to a competition between the N_2 reduction reaction and the H_2 evolution reaction. An elegant tandem catalytic strategy recently proposed to circumvent this problem involves use of a co-catalyst capable of mediating a H atom transfer to a N_2-bonded metal center (Chatt-like complex), reaching 40 TON at most.[28–30] The same group reported in 2023 that the complex $[(^{H}PNP)MoBr_3]$ can

be used to achieve the conversion of dinitrogen into ammonia under electrocatalytic conditions. The authors showed that a controlled potential electrolysis carried out at − 1.89 V (*vs*. Fc^+/Fc) on a Boron Doped Diamond (BDD) electrode in the presence of 100 molar equivalents of collidinium triflate in THF/LiTFSI affords up to 11.7 equivalents of ammonia per Mo atom.[29] It should also be pointed out that these performances are similar to those obtained in 2011 by Nishibayashi et al. when studying the chemical reduction of [(HPNP)$MoCl_3$] using lutidinium triflate (100 eq.) and Cp_2Co (72 eq.) as proton and electron sources.[31] Electrochemical approaches involving molecular catalysts thus remain to be explored. The handful of examples cited above highlight the feasibility and great potential of such approach aiming at improving the efficiency of the conversion and at avoiding use of non-selective reducing agents. Designing selective/robust catalysts is thus required to achieve the binding and reduction of N_2 at low potentials and with high Faradaic efficiency (FE).

This study is built on our recent discovery of the first synthesis of borylamine from mixtures of N_2, Cy_2BCl and K using a (PPP)Mo complex as a catalyst.[6] We report here the electrochemical reduction of N_2 into borylamine using Cy_2BCl as an electrophile and the Mo≡N complex [$\mathbf{1}^{IV}$] as a catalyst (Scheme 1). The catalytic process and the species involved in the cycle have been identified on the ground of in-depth spectroscopic and electrochemical studies. In particular, our studies have revealed the crucial role of in-situ generated protons in the catalytic cycle.

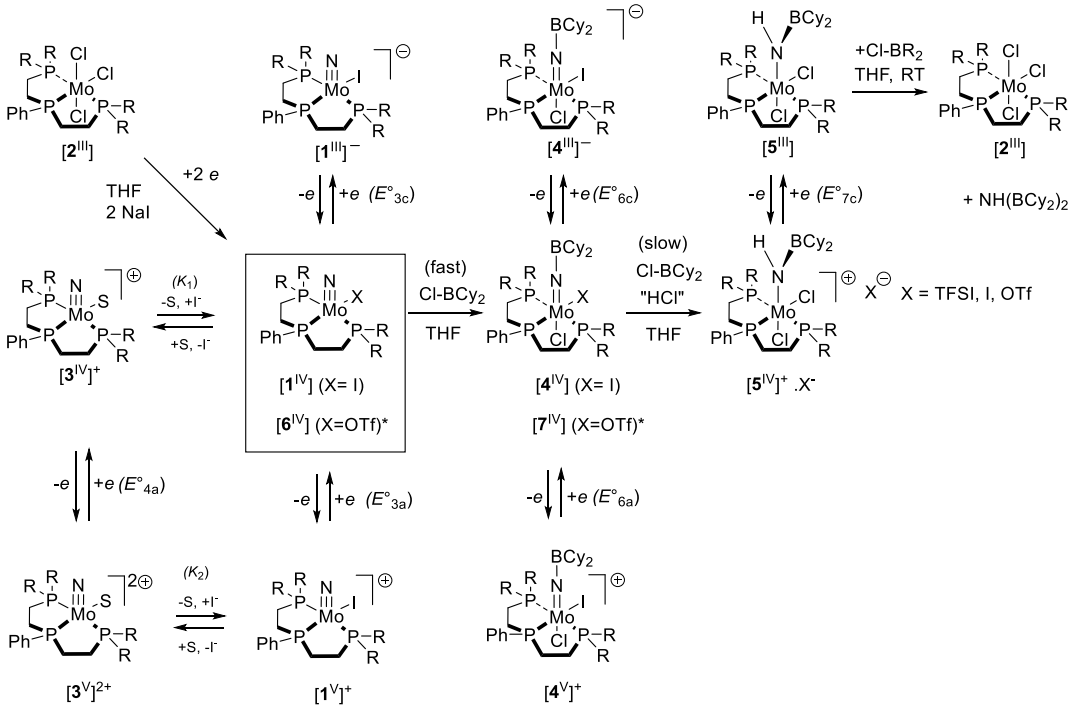

Scheme 1. Reactivity of complex [**1**^{IV}] triggered by electron transfer or addition of Cy_2BCl on the Mo≡N bond (*species considered as models in our DFT studies).

Results and Discussion

The nitrido complex [($P^{Ph}P_2^{Cy}$)Mo(≡N)(I)] ([$\mathbf{1}^{IV}$] in Scheme 1) was synthesized in one step using a previously reported procedure, proceeding through a Na(Hg)-mediated two electron chemical reduction of the chlorinated precursor [($P^{Ph}P_2^{Cy}$)$MoCl_3$] ([$\mathbf{2}^{III}$] in Scheme 1) in the presence of N_2 and NaI, followed by a spontaneous splitting of the in situ generated Mo-N≡N-Mo intermediate.[26] The reactivity of the nitrogen atom in [$\mathbf{1}^{IV}$] towards Cy_2BCl was already studied by us in pure THF.[6] This study was therefore extended to electrochemical conditions, with the electrochemical behavior of [$\mathbf{1}^{IV}$] and [$\mathbf{4}^{IV}$] being studied in greater detail in the present manuscript.

As a starting point, the electrochemical signature of the [$P^{Ph}P_2^{Cy}$PMo(≡N)(I)] complex [$\mathbf{1}^{IV}$] was investigated by cyclic voltammetry (CV) measurements carried out in THF in the presence of tetra-*n*-butylammonium bis-trifluoromethanesulfonimidate (TBA.TFSI).[6] As can be seen in Figure 1A, the CV curves recorded at a glassy carbon (GC) working electrode display a Nernstian one-electron oxidation wave at $E_{1/2}$ = – 0.71 V and two fully irreversible waves below – 2.7 V.

The oxidation wave attributed to the one-electron oxidation of the $Mo^{(IV)}$ center proved reversible at all investigated scan rates, *ie* from 50 to 2000 $mV.s^{-1}$. The diffusion coefficient of [$\mathbf{1}^{IV}$] was estimated at $2.21x10^{-5}$ $m^2.s^{-1}$ using the Cottrel equation (Figure S1) and the number of electrons exchanged in this oxidation wave was ascertained by exhaustive electrolysis (see below). The first irreversible reduction wave observed at E_p = – 2.9 V was attributed to the one electron reduction of the $Mo^{(IV)}$ center yielding an unstable $Mo^{(III)}$ complex readily transformed into a species most likely reduced at lower potentials. Addition of tetra-*n*-butylammonium iodide in excess to an electrolytic solution of [$\mathbf{1}^{IV}$] was found to result in a shift of about 70 mV of the reversible Mo-centered oxidation wave (Figure S2), supporting the idea that there is a fast exchange in solution between [$\mathbf{1}^{IV}$] [($P^{Ph}P_2^{Cy}$)Mo(≡N)(I)] and [$\mathbf{3}^{IV}$]$^+$ [($P^{Ph}P_2^{Cy}$)Mo(≡N)(THF)]$^+$ (K_1 in Scheme 1), and that the signal recorded in these condition is an average picture of the square scheme involving [$\mathbf{1}^{IV}$] / [$\mathbf{1}^{V}$]$^+$ and [$\mathbf{3}^{IV}$]$^+$ /[$\mathbf{3}^{V}$]$^{2+}$.

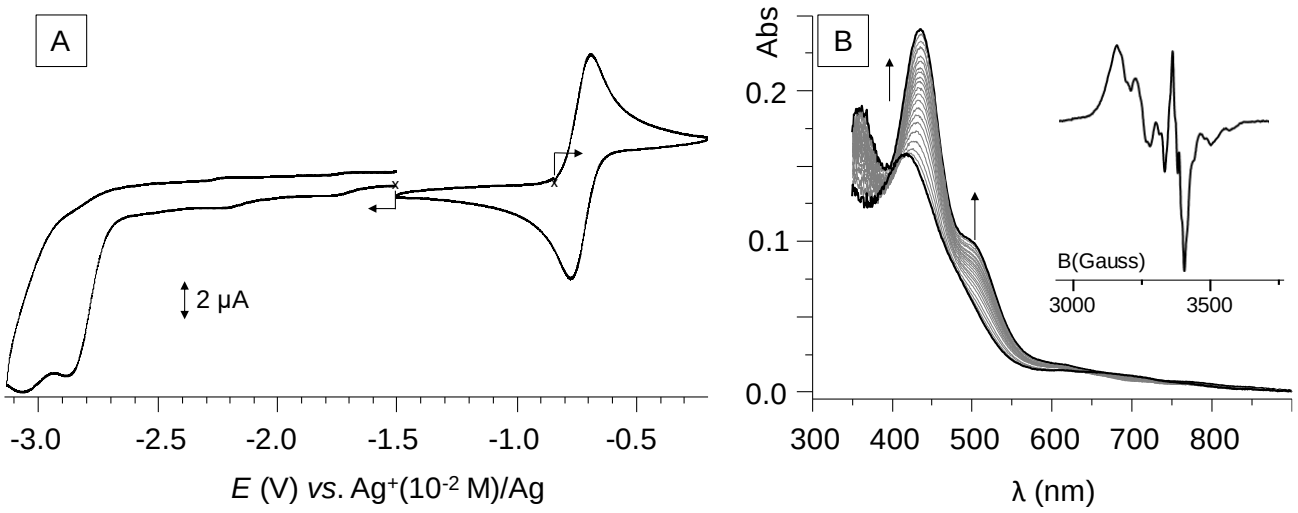

Figure 1. A) Cyclic voltammograms of [**1**^{IV}] (1 mM in THF + 0.1 M TBA.TFSI). Scan rate: 100 mV.s^{-1}; working electrode: GC (∅ 3 mm); counter electrode: Pt wire; reference: $AgNO_3$ (10^{-2} M)/Ag. B) UV/vis absorption spectra recorded during the exhaustive electrolysis of [**1**^{IV}] (1 e$^-$/mole, 1 mM in THF + 0.1 M TBA.TFSI; Pt grid, E_{app} = – 0.5 V, 5 mL, l = 1 mm, t ≈ 1 h). Inset ESR spectrum recorded in THF + TBA.TFSI (0.1 M) at 110 K.

Further studies revealed that the Mo^V complex [**1**^{V}]$^+$, generated in situ by exhaustive one electron-oxidation of [**1**^{IV}] at – 0.5 V *vs*. *E*[Ag$^+$/Ag] in THF, is stable in solution at the electrolysis time scale (hour). The advancement of the oxidation was followed by UV-vis absorption measurements and the stability of [**1**^{V}]$^+$ was demonstrated by CV and rotating disk voltammetry measurements (see Figure S3). As can be seen in Figure 1B, the accumulation of [**1**^{V}]$^+$ resulted in a significant bathochromic and hyperchromic shift of the main absorption band observed in the visible range, *ie* from λ_{max} = 418 to 436 nm with an intensity gain of + 65 %, and in the development of a shoulder at 500 nm. ESR spectroscopy data collected before and after the one electron oxidation of [**1**^{IV}] also confirmed our attribution, the silent ESR spectrum recorded for the starting Mo^{IV} complex (d^2, S = 0, Figure S15) evolving after oxidation into intense signals consistent with the formation of Mo^V (d^1, S = ½) species (inset of Figure 1B, for simulation details, see Figure S14 and Table S1).

In a second stage, we probed the impact of the presence of an electrolyte on the chemical transformation of [$\mathbf{1}^{IV}$] to [$\mathbf{4}^{IV}$]. As in pure THF, the targeted complex [$\mathbf{4}^{IV}$] [($P^{Ph}P_2^{Cy}$)Mo^{IV}(=$NBCy_2$)(I)(Cl)] (Scheme 1) was formed quickly and quantitatively in THF + TBA.TFSI (0.1 M ≈ 100 molar eq.) upon addition of one molar equivalent of Cy_2BCl. This transformation was moreover confirmed by ^{31}P NMR spectroscopy measurements, with the appearance of two singlets at 102.3 and 61.9 ppm, and by spectrophotometry measurements though the progressive development of a band centered at λ_{max} = 395 nm, these two sets of data being characteristic signatures of the imido complex [$\mathbf{4}^{IV}$] (Figure S16, S17 and S19).[6]

Turning to electrochemical methods, the addition of Cy_2BCl to a solution of the nitrido complex [$\mathbf{1}^{IV}$] in THF/TBA.TFSI led to a clean "two waves" type of conversion (Figure 2A), including a progressive decrease in the intensity of the initial wave attributed to the one electron oxidation of [$\mathbf{1}^{IV}$] ($E°_{3a}$ in Scheme 1) in favor of another reversible wave centered at $E_{1/2}$ = – 0.35 V, reaching a maximum intensity after addition of one molar equivalent of Cy_2BCl.[6] The anodic shift of more than 370 mV from the initial wave is consistent with a decrease in the electron density at the Mo(IV) center under the effects of the conversion of the nitrido ligand into a boryl imido ligand. This supports the attribution of the latter wave to the one-electron oxidation of the in situ generated imido complex [($P^{Ph}P_2^{Cy}$)Mo^{IV}(=$NBCy_2$)(I)(Cl)] ([$\mathbf{4}^{IV}$]→[$\mathbf{4}^{V}$]$^+$ in Scheme 1). The first oxidation centered on [$\mathbf{4}^{IV}$] is followed by another fully irreversible wave of much weaker intensity at E_p = 0 V which could be readily assigned to the oxidation of free iodide anions released in situ (see Figure S4). The intensity of this iodide-centered oxidation wave was also seen to increase with scan rate, consistent with a chemical reaction independent of the oxidation of [$\mathbf{4}^{IV}$] (Figure S5). As already explained when discussing the CV curves of [$\mathbf{3}^{IV}$], the release of iodide from [$\mathbf{4}^{IV}$] is explained by the use of a solvent with a quite significant coordinating power and by the weak and labile character of the Mo-I bond which happens to be quite long, as previously established on the ground of X-ray diffraction data.[6]

As expected for electron transfer centered on the same fragment of the molecule, the addition of Cy_2BCl was found to result in similar anodic shift of the wave observed on the cathodic side, with a new

irreversible wave developing at E_p = – 2.5 V attributed to the reduction of the Mo center in the imido complex ([**4**^{IV}]/[**4**^{III}]$^{-}$), followed by a coupled chemical reaction. As can be seen in Figure 2B, this first fully irreversible reduction process is then followed by a second irreversible reduction wave at E_p = – 2.9 V which happens to be very similar, albeit slightly cathodically shifted (ΔE_p = 34 mV), to that observed on the CV curve of the initial nitrido complex ([**1**^{IV}]/[**1**^{III}]). The intensity of the irreversible reduction wave at E_p = – 2.5 V was however seen to increase with scan rate at the expense of the following reduction wave at E_p = – 2.9 V (see Figure S6), a behavior consistent with a second reduction event linked to the reduction wave at E_p = – 2.5 V. These results thus led us to assign the wave at E_p = – 2.5 V to a Mo^{IV}/Mo^{III} reduction and the following wave at E_p = – 2.9 V to a reduction of an in situ generated species.

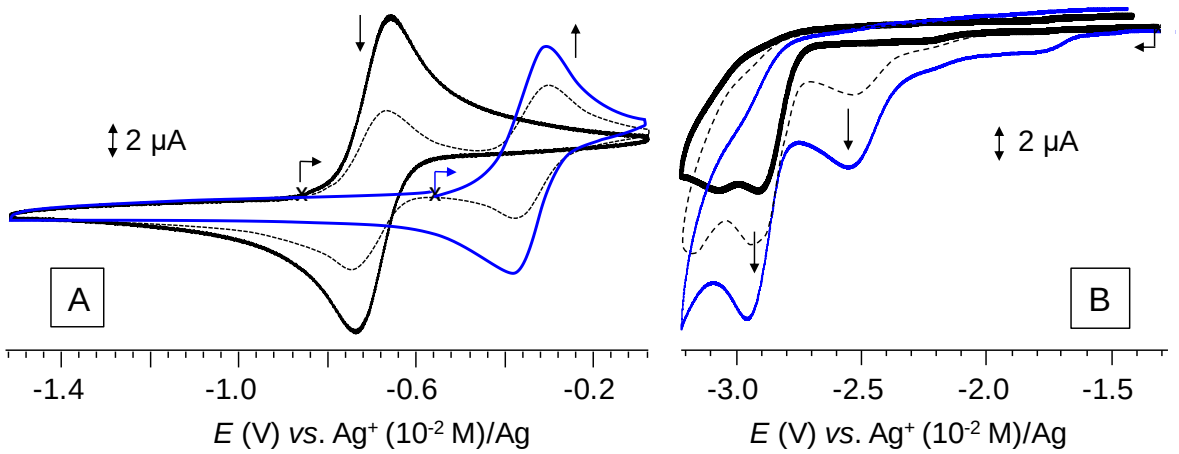

Figure 2. Cyclic voltammograms recorded for a 1 mM solution of [**1**^{IV}] in THF + TBA.TFSI (0.1 M) after addition of 0 (solid black line), 0.5 (dashed line) and 1 (solid blue line) molar equivalent of Cy_2BCl (1 M in hexane) in oxidation (A) and reduction (B). Scan rate: 100 mV.s^{-1}. WE in GC (∅ 3 mm), CE in Pt, reference: $AgNO_3$(10^{-2} M)/Ag.

The ability of the reduced form of [($P^{Ph}P_2^{Cy}$)Mo(≡N)(I)] [**1**^{IV}] to promote the reduction of nitrogen in presence of Cy_2BCl was then evaluated under catalytic conditions using TBA.TFSI/THF as an electrolyte and Cy_2BCl in excess. The curves shown in Figure 3, recorded after addition of 1 and 30 molar equivalents of Cy_2BCl to a solution of [**1**^{IV}] in the presence of electrolyte bring to light the development of an intense

wave at E_p = – 2.35 V attributed to the electrocatalytic reduction of Cy_2BCl. The catalytic role of the Mo center in this process was further demonstrated by the large anodic shift (+700 mV) of the wave attributed to the reduction of Cy_2BCl in the presence of [$\mathbf{1}^{IV}$] (see dashed and solid black lines in Figure 3).

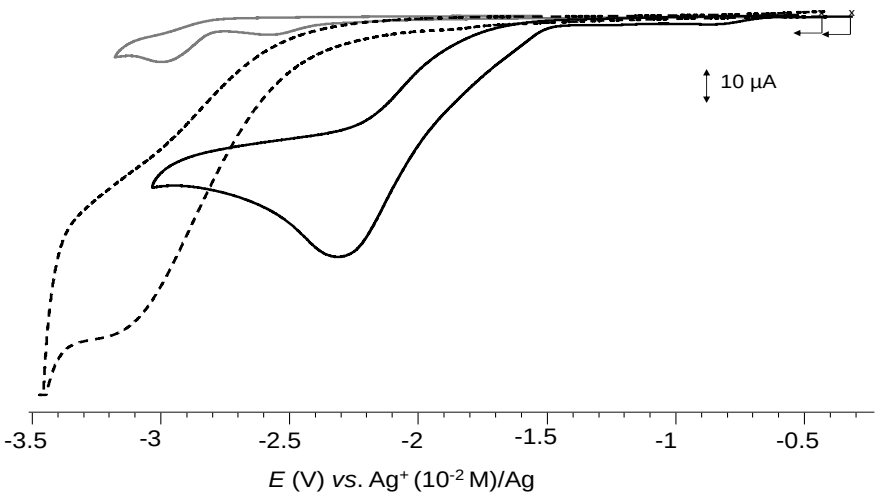

Figure 3. Cyclic voltammograms of [$\mathbf{1}^{IV}$] (1 mM in THF + TBA.TFSI) recorded after addition of 1 molar eq. of Cy_2BCl (solid grey line) and 30 molar eq. of Cy_2BCl (solid black line). The CV curve recorded for a solution of Cy_2BCl alone (30 molar eq. in THF + TBA.TFSI) is shown as a black dashed line. Scan rate: 100 $mV.s^{-1}$. WE in GC (∅ 3 mm), CE in Pt, reference: $AgNO_3$(10^{-2} M)/Ag.

On the ground of these observations, electrolysis were then conducted at room temperature inside an N_2-regulated glove box using a home-made divided cell and a glassy carbon foam working electrode. All experiments were carried out under potentiostatic conditions and followed by coulometry measurements. The efficiency of the reduction process was assessed from the amount of NH_4^+ produced after submitting the electrolyzed samples to hydrolysis (see SI section for details). Several parameters were tested including the [$\mathbf{1}^{IV}$]:Cy_2BCl ratio (1:30 or 1:60) and the potential value applied at the working electrode (– 2.3 to – 3.2 V, entry 1-5). In each case, electrolysis was carried out until a maximum charge was reached (5.6 to 6.5 C for 30:1 ratio, Table 1). These studies revealed that the applied potential has a major effect on the overall yield spanning from 12 to 38 % for the 30:1 mixture. We also found that an increase in the concentration of Cy_2BCl is detrimental, as revealed by a large drop in the conversion yield (from

38 to 6 % yield, see Table 1, entries 3 *vs* 7). In support of the key role of the Mo center, we found that a control electrolysis performed without [**1**^{IV}] (Table 1, entry **6**) produced no NH_4^+. These results thus show that the chemical and electrochemical reduction conditions used so far lead to radically different results. We have indeed previously shown that the chemical reduction of Cy_2BCl by K generates Cy_2B radicals which react with N_2 to produce NH_4^+ after hydrolysis.[32] The control experiments discussed above thus show that such Cy_2B radicals are not produced under the electrochemical conditions used here. We also found that the reaction carried out under an argon atmosphere with complex [**1**^{IV}] (Table 1, entry **8**) gave 0.6 equiv. of NH_4^+, which corresponds to the amount obtained after direct hydrolysis of complex [**1**^{IV}] (see Figure S30 showing the quantification of NH_4^+ obtained after treatment of [**1**^{IV}] with an excess of HCl).

The influence of the applied potential (E_{app}) on the Mo-catalyzed reduction of N_2 is best revealed by the volcano plots depicted in Figure 4, showing a rapid increase in the efficiency markers (FE or TON) with increasing E_{app} to a maximum reached at – 2.7 V, followed by a decrease attributed to a loss in the selectivity of the reduction process. These results nevertheless bring to light that the catalytic process is linked to the reduction wave observed in Figure 3. The catalytic nature of the process is also demonstrated by the TON values, with a maximum of ~ 4 equivalents of NH_4^+ per Mo center, and by control experiments carried out under argon giving sub stoichiometric amounts of NH_4^+ (entry 8 in Table 1).

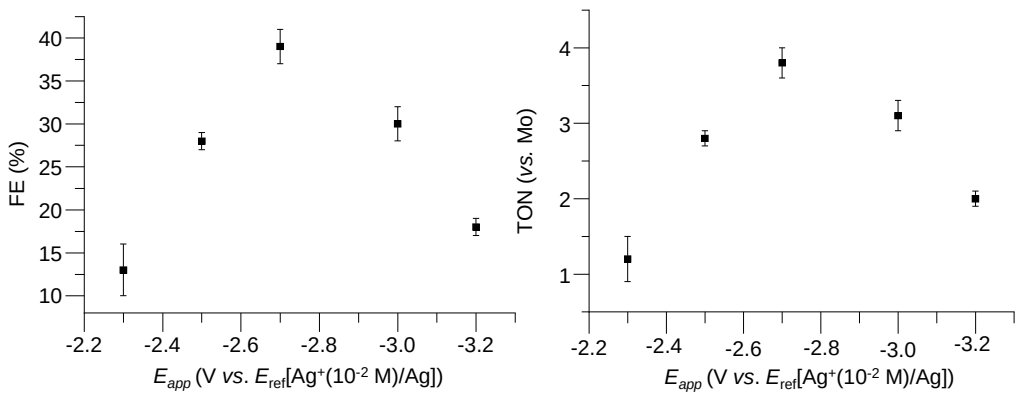

Figure 4. volcano plot of FE and TON versus applied potential. Data calculated from the amount of NH_4^+ produced after electrolysis of [**1**^{IV}] (1mM) + Cy_2BCl (30 mM) in THF + TBA.TFSI (0.1 M). Potential

applied versus $E[Ag^+ (10^{-2}\ M)/Ag]$, WE in GC foam, CE in carbon graphite, reference electrode: $AgNO_3$ $(10^{-2}\ M)/Ag$).

Table 1. Electrocatalytic results. Standard conditions: catalyst (1 mM), 20 °C, THF TBA.TFSI: 0.1 M (2 mL), potential applied versus $AgNO_3$ $(10^{-2}$ M)/Ag, working electrode: glassy carbon foam, counter electrode: carbon in acetonitrile/DMF TBA.TFSI, reference electrode: Ag^+ $(10^{-2}$ M)/Ag. yield, FE and TON are the average of 2 experiments (standard variation given). TON is defined as the amount of NH_4^+ per amount of complex; yield = $3n(NH_4^+)/n(Cy_2BCl)$; FE = $3n(NH_4^+)F/Q$, where $n(NH_4^+)$ and $n(Cy_2BCl)$ are the amount of moles of ammonium and chloroborane, F the Faraday's constant and Q the charge passed. a) controlled potential electrolysis performed under an N_2 atmosphere. b) controlled potential electrolysis performed under an Ar atmosphere.

Ent.	TBATFSI	Cy_2BCl : [1^{IV}]	E_{app} (V)	Charge (C)	Yield (%)	FE (%)	TON
1[a]	**0.1 M**	30 : 1	– 2.3	– 5.6	12 ± 3	13 ± 3	1.2 ± 0.3
2[a]	**0.1 M**	30 : 1	– 2.5	– 5.8	28 ± 1	28 ± 1	2.8 ± 0.1
3[a]	**0.1 M**	30 : 1	– 2.7	– 5.7	38 ± 2	38 ± 2	3.8 ± 0.2
4[a]	**0.1 M**	30 : 1	– 3.0	– 6.0	31 ± 2	30 ± 2	3.1 ± 0.2
5[a]	**0.1 M**	30 : 1	– 3.2	– 6.5	20 ± 1	18 ± 1	2.0 ± 0.1
6[a]	**0.1 M**	30 : 0	– 2.7	– 5.5	0	0	0
7[a]	**0.1 M**	60 : 1	– 2.7	– 10.9	6 ± 0.2	6 ± 0.2	1.3 ± 0.02
8[b]	**0.1 M**	30 :1	– 2.7	– 6.0	6 ± 1	6 ± 1	0.6 ± 0.1

In-depth analytical studies were then undertaken to decipher the catalytic mechanism. Our first studies presented above have clearly established that the starting point of the mechanism is the formation of [$\mathbf{4}^{IV}$]. We have then studied the evolution of that species after adding an excess of Cy_2BCl in the presence of TBA.TFSI, *i.e.* in the conditions of the electrocatalytic process. UV-visible absorption measurements conducted after addition of 30 molar equivalents of Cy_2BCl revealed the conversion of the band centered at 395 nm in favor of a new signal developing at 344 nm (Figure S18), which is consistent with a slow

conversion of [**4**^{IV}]. It should be noted that [**4**^{IV}] proved stable in pure THF in the presence of an excess of Cy_2BCl and that the consumption/reaction of [**4**^{IV}] was only observed in electrolytic conditions. Here again, this result points to major mechanistic differences between the chemical and electrochemical activation pathways and to the key role of the electrolyte.

As a matter of fact, this result echoes previous studies showing that increased reactivity of boryl or silylimido complexes towards electrophiles can be mediated by iodide abstraction from the Mo coordination sphere.[33] As demonstrated by the observation of an iodide oxidation wave in the CV curve of [**4**^{IV}], the electrolyte promotes a dissociation of the Mo-I bond to form a reactive cationic intermediate $[(P^{Ph}P_2{}^{Cy})Mo^{IV}(=NBCy_2)(Cl)]^+$. Subsequent addition of a second equivalent of Cy_2BCl was expected to form a bis(boryl)amido complex $[(P^{Ph}P_2{}^{Cy})Mo^{IV}(N(BCy_2)_2)Cl_2]^+$, as observed for related complexes and reactants.[26,33,34]

DFT calculations (see Scheme S1) were carried out to explain the observed reactivity and to identify the reactions triggered by addition of an excess Cy_2BCl. These computational studies were conducted with the nitrido triflate complex [**6**^{IV}] (Scheme 1), chosen as a model of the in situ generated "iodide-free" complexes.[33] The first addition of Cy_2BCl yielding complex [**7**^{IV}] $[(P^{Ph}P_2{}^{Cy})Mo^{IV}(NBCy_2)(OTf)(Cl)]$ was computed exergonic (-13.5 kcal mol^{-1}). The addition of a second equivalent of Cy_2BCl, leading to the initially foreseen bis borylamido cationic complex [**11**^{IV}]$^+$ $[(P^{Ph}P_2{}^{Cy})Mo^{IV}(N(BCy_2)_2)Cl_2]^+$, was conversely found to be endergonic (ΔG = 6.7 kcal mol^{-1} with respect to [**7**^{IV}], the triplet state for [**11**^{IV}]$^+$ being more stable than singlet by 11.3 kcal/mol). This led us to conclude that such species does not form in our experimental conditions. On the other hand, the 1,2 addition of HCl on the Mo=N bond in [**7**^{IV}] affords the borylamido cationic complex [**5**^{IV}]$^+$ $[(P^{Ph}P_2{}^{Cy})Mo^{IV}(NHBCy_2)Cl_2]^+$ in a strongly exergonic manner (– 19.6 kcal mol^{-1} *vs* [**7**^{IV}]; – 33.1 kcal mol^{-1} *vs* [**6**^{IV}]), with complex [**7**^{IV}]$^+$ being more stable in the triplet state than in the singlet state (by *ca* 15 kcal/mol). These results are also in full agreement with experimental UV-vis abs. data showing that the signals attributed to the borylimido complex [**4**^{IV}] disappear over time in the presence of an excess of Cy_2BCl and electrolyte. Numerous experimental

studies were then carried out to identify the unexpected source of protons in the mixture. In the absence of water, Cy_2BCl is stable in THF, affording a simple adduct easily identified by ^{11}B NMR spectroscopy (22 ppm in THF *vs* 73 ppm in hexanes).[35] It is however known that strong Lewis acids such as dialkylboron triflates and iodides react with THF to yield ring opened species and protons.[35]

This known reactivity led us to consider that the "free" iodide anions released from the Mo center in the presence of electrolyte (see K_1 in Scheme 1) could be involved in an exchange reaction with chloroborane producing in situ an iodoborane capable of opening THF and releasing protons (Scheme 2A). This assumption has first been confirmed upon showing that the addition of stoichiometric amounts of TBAI to a solution of Cy_2BCl in THF results in a quantitative transformation of the B-Cl bonds into B-OR, as revealed by the appearance of a signal at 53 ppm in the ^{11}B NMR spectrum of the mixture. The presence of protons was then revealed by subsequent addition of NEt_3 in the mixture leading to the precipitation of $NEt_3H^+ X^-$ (X = Cl or I), easily identified by ^1H NMR spectroscopy measurements (Figure S20 to S26).

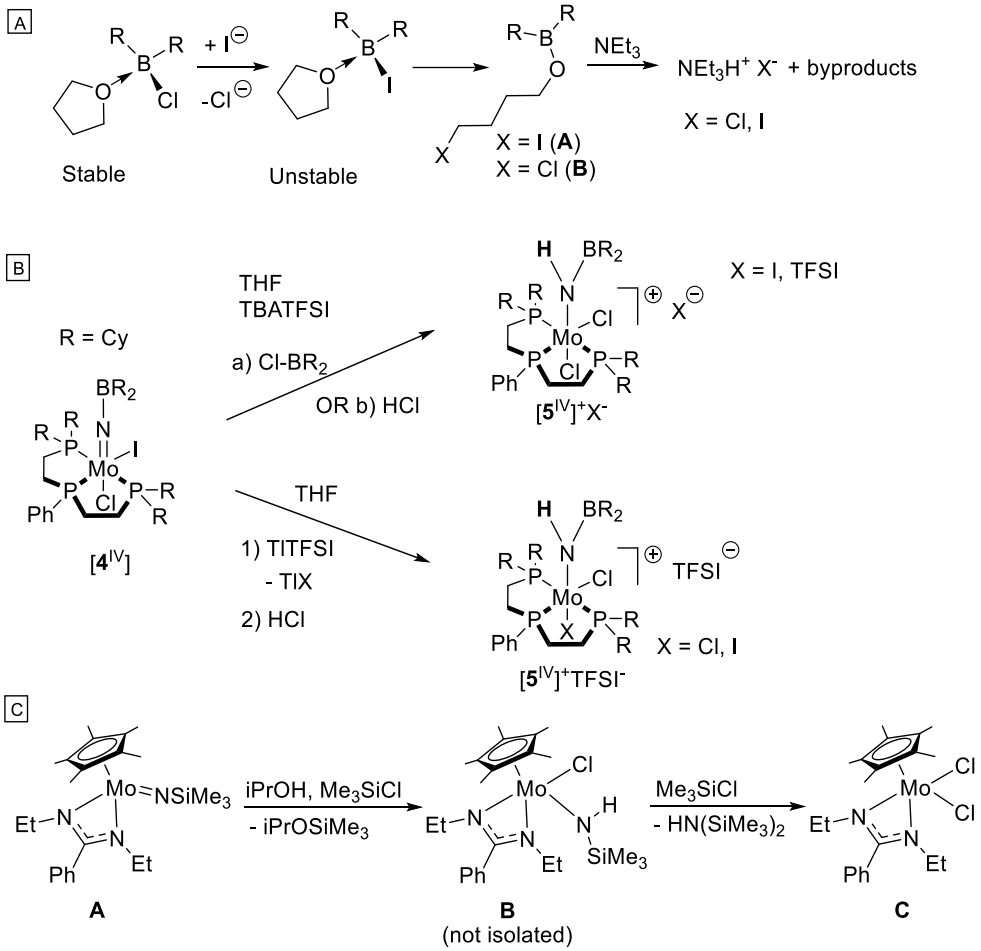

Scheme 2. Proposed mechanistic and synthetic pathways for A) opening of THF with release of acid and B) conversion of borylimido complex [**4**^{IV}] to cationic boryl-amido [**5**^{IV}]$^{+}$ formed in electrochemical conditions (*i.e.* excess of Cy_2BCl or HCl in THF TBATFSI 0.1 M) or chemical conditions (*i.e.* abstraction of the iodo ligand with TlTFSI) in THF at RT. C) protonation of the silylimido complex A with iPrOH and Me_3SiCl.[36]

Further evidence of the in situ formation of protons in the reaction mixture was obtained by comparing the CV curves recorded after addition of Cy_2BCl or HCl to an electrolytic solution of [**1**^{IV}] in THF. As can be seen in Figure 5, the curves recorded after addition of more than 2 eq. of Cy_2BCl , or 1 eq. Cy_2BCl and 2 eq. HCl, exhibit the same characteristics, namely i) disappearance of the reversible wave at $E_{1/2}$ = – 0.35 V attributed to the oxidation of the in situ generated borylimido complex [**4**^{IV}], ii) development of an irreversible oxidation wave at 0 V, confirming the presence of free iodide in the mixture, and iii)

development of another irreversible reduction wave at $E_p = -0.78$V attesting to the formation of the same species $[\mathbf{5}^{IV}]^+$ in both conditions.

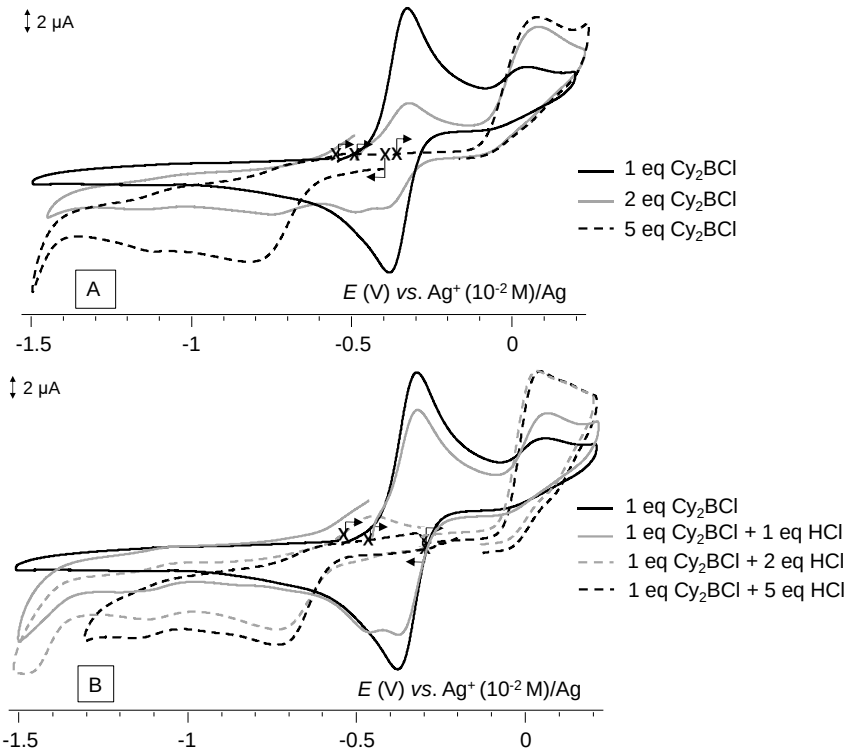

Figure 5. A) Cyclic voltammograms recorded for a 1mM solution of $[\mathbf{1}^{IV}]$ in THF + TBA.TFSI (0.1 M) after addition of x molar equivalents (eq.) of Cy_2BCl (x = 1, solid black; x = 2 solid grey; x = 5 dotted black). B) Cyclic voltammograms recorded for a 1mM solution $[\mathbf{1}^{IV}]$ in THF + TBA.TFSI (0.1 M) after sequential addition of 1 eq. of Cy_2BCl and then x eq. of HCl (x= 0 solid black; x = 1 solid grey; x = 2 dotted grey; x = 5 black). Scan rate: 100 mV.s^{-1}. Working electrode: GC (∅ 3 mm), counter electrode: Pt, reference: Ag^+ (10^{-2} M)/Ag.

All together, these experiments demonstrate the in situ formation of H^+, thus providing a low energy pathway to a conversion of the imido complex $[\mathbf{4}^{IV}]$ into the protonated boryl-amido complex $[\mathbf{5}^{IV}]^+$ $[(P^{Ph}P_2{}^{Cy})Mo^{IV}(NHBCy_2)Cl_2]^+$ (Scheme 2B). It should be noted that a related behavior was observed by Sita *et al.* when studying the silylimido complex **A**, (Scheme 2C). The latter complex, which was initially found to be non-reactive towards $SiMe_3Cl$, could eventually be converted to the silylamido complex **B** by reaction with HCl generated in situ from a mixture of TMSCl and isopropyl alcohol (3:1). This intermediate complex could however not be isolated, as it readily evolved in the presence of TMSCl into complex **C** with liberation of the corresponding bis-silylamine.[36]

Attempts to isolate complex $[\mathbf{5}^{IV}]^+$ from the electrochemical medium proved impossible. We have thus set up a chemical synthetic strategy to generate the proposed cationic boryl-amido complex. The first step of the sequence, detailed in scheme 2B, involves abstraction of the coordinated halides from the borylimido complex $[\mathbf{4}^{IV}]$ using TlTFSI. This reaction afforded a cationic borylimido complexes ($^{31}P\{^1H\}$ and ^1H spectra shown in Fig. S33 et S34), coming along with precipitation of TlCl/TlI. Subsequent addition of 1.0 equivalent of HCl (1M in Et_2O) resulted in a loss of the $^{31}P\{^1H\}$-NMR signals and in the low-field shift and broadening of the ^1H-NMR signals, attesting formation of paramagnetic species. These experimental data, together with the DFT calculations presented above, are thus fully consistent with the formation of the desired paramagnetic complex $[\mathbf{5}^{IV}]$TFSI. Cyclic voltammetry measurements realized on this complex (Figure S8 and S9) display several irreversible reductions at E_p = – 0.76, – 1.1 V, – 1.7 V and – 2.9 V identical to $[\mathbf{5}^{IV}]^+X^-$ formed in electrochemical conditions (*i.e.* excess of Cy_2BCl or HCl in THF TBATFSI 0.1 M, see Figure 5 and Figure S8, X =I or TFSI), fully supporting its formation in solution.

We then focused on the chemical steps coupled to the one-electron reduction of $[\mathbf{5}^{IV}]^+$, formed in situ in the presence of an excess of Cy_2BCl. The CV of $[\mathbf{5}^{IV}]^+$ exhibits several consecutive irreversible reduction waves, at E_p = – 0.78, – 1.12 and – 1.71 V (see Figure S7). We hypothesized that the electrogenerated Mo(III) center in $[\mathbf{5}^{III}]$, unlike $[\mathbf{5}^{IV}]^+$, could further reacts with Cy_2BCl to afford the trichloro Mo^{III} complex $[\mathbf{2}^{III}]$ together with $NH(BCy_2)_2$ (Scheme 1). This assumption was eventually confirmed by showing that the CV curve of $[\mathbf{2}^{III}]$ $[(P^{Ph}P_2{}^{Cy})MoCl_3]$,[8,26] exhibits one fully irreversible reduction wave at E_p = – 1.71 V matching that observed on the CV of mixtures of $[\mathbf{5}^{IV}]^+$ and Cy_2BCl (see Figure S7). Moreover, ^1H and $^{15}N/^1H$ HSQC NMR measurements conducted on the unpurified mixture obtained after electrolysis carried out under the conditions of entry 3 (Table 1) demonstrated the formation of $NH(BCy_2)_2$ (see Figure S27 and S28).

Having demonstrated HCl production from $Cy_2BCl/THF/I^-$ mixtures, we set up experiments to determine whether complex $[(P^{Ph}P_2{}^{Cy})Mo(\equiv N)(I)]$ $[\mathbf{1}^{IV}]$ could also act as a catalyst for NH_3 production, possibly

followed by a reaction between NH_3 and Cy_2BCl to generate the observed product $NH(BCy_2)_2$. This hypothesis was first verified by studying the electrochemical behavior of complex [$\mathbf{1}^{IV}$] in the presence of HCl. As can be seen in Figure S10 and S11, the addition of proton in the electrochemical cell leads to the observation of intense signals most likely attributed to the direct or indirect reduction of protons. We also found that the electrolysis of [$\mathbf{1}^{IV}$] carried out in THF (+ 0.1 M TBATFSI) at E_{app} = – 2.7 V (– 3.2 C) in the presence of HCl (5 molar eq.) produces less than 0.5 molar equivalent of ammonia (Figure S29). In a second series of experiments, we also found that $NH(Cy_2B)_2$, the only product obtained after the electrolyses carried out under the conditions shown in Table 1, is not produced when NH_3 and Cy_2BCl are just mixed in THF (see boron NMR and ^{15}N-^{1}H HMBC spectra in figure S29-30).

Taken together, these control experiments therefore demonstrate that the formation of $NH(Cy_2B)_2$ observed under our electrolysis conditions requires first reaction of the Mo≡N bond with Cy_2BCl to generate the boryl imido intermediate [$\mathbf{4}^{IV}$]. Only then is I^- decoordinated from the Mo center, leading to H^+ formation from Cy_2BCl/THF.

To complete the catalytic cycle, we then checked whether the reduction of [$\mathbf{2}^{III}$] [$(P^{Ph}P_2^{Cy})MoCl_3$] in the presence of N_2 could potentially regenerate the starting nitride complex [$\mathbf{1}^{IV}$] [$(P^{Ph}P_2^{Cy})Mo(\equiv N)(I)$], which is actually quite a complex process, or its chloride analog [$(P^{Ph}P_2^{Cy})Mo(\equiv N)(Cl)$]. Previous works focusing on chemical reduction approaches have shown that NaI has to be used in conjunction with [$(P^{Ph}P_2^{Cy})MoCl_3$] to enable the efficient formation of [$(P^{Ph}P_2^{Cy})Mo(\equiv N)(I)$] (yield of *ca* 80 % estimated by ^{31}P NMR).[37] Other studies have also established that [$(P^{Ph}P_2^{Cy})Mo(\equiv N)(I)$] can be obtained with *ca* 30 % yield and 49 % FE as product of the electrochemical reduction of [$(P^{Ph}P_2^{cy})MoI_3$].[38]

In our experimental conditions, CV measurements conducted with [$\mathbf{2}^{III}$] [$(P^{Ph}P_2^{Cy})MoCl_3$] showed that the fully irreversible reduction at E_p = – 1.7 V produces a new species (Figure S12), [$\mathbf{10}^{IV}$]$^-$ (*vide infra*), which gets reoxidized at E_p = – 0.72 V, a value which happens to be similar to that expected for the oxidation of [$\mathbf{1}^{IV}$] (*vide supra*). Exhaustive electrolysis of a 1mM solution of [$\mathbf{2}^{III}$] in THF (0.1 M TBA.TFSI) under N_2 at E_{app} = – 1.85 V was performed, (Figure 6A), requiring 2 electrons per mole of

[$\mathbf{2}^{III}$]. The CV curves recorded after completion of the reduction was found to exhibit one irreversible oxidation wave at E_p = – 0.72 V. These results are thus fully consistent with the reaction of the electrogenerated complex [($P^{Ph}P_2^{Cy}$)Mo(Cl)] with N_2 to afford the nitrido complex [($P^{Ph}P_2^{Cy}$)Mo(N)(Cl)] [$\mathbf{9}^{IV}$] via N_2 splitting, in a similar fashion than [($P^{Ph}P_2^{Cy}$)Mo(I)]. Differences were however observed in the two cases. Indeed, the irreversibility of the oxidation wave shown as a solid gray line in Figure 6A contrasts with the reversible signal observed with [$\mathbf{1}^{IV}$]. It could be attributed to the absence of iodide and to the presence of chlorides in the electrolyzed mixture ([($P^{Ph}P_2^{Cy}$)$MoCl_3$], TBA.TFSI, THF). This hypothesis was validated upon studying the influence of chlorides on the electrochemical signature of [$\mathbf{1}^{IV}$] [($P^{Ph}P_2^{Cy}$)Mo(≡N)(I)].

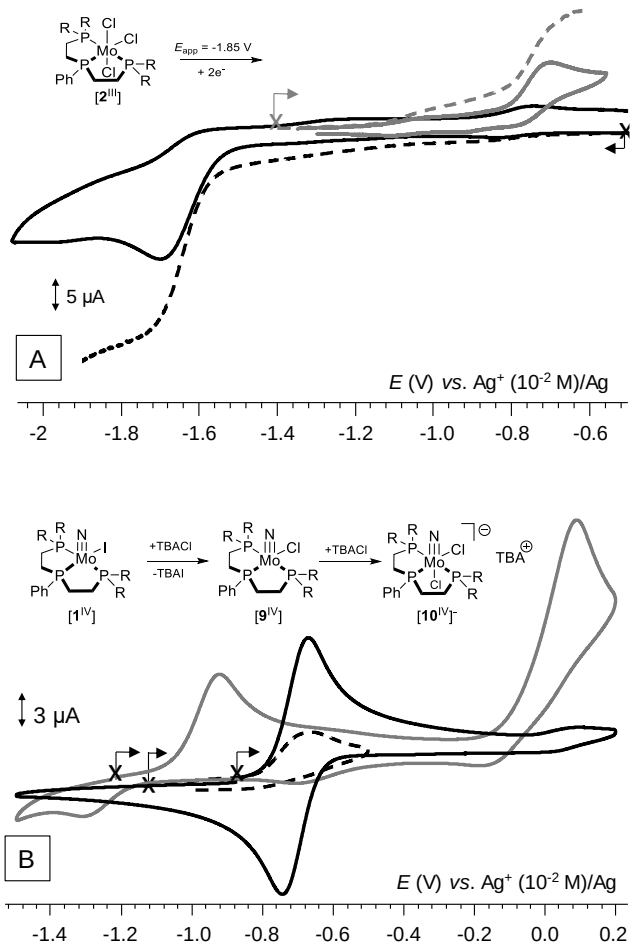

Figure 6. A) Voltammograms of [$\mathbf{2}^{III}$] (1 mM in THF + TBA.TFSI (0.1 M)) before (black trace) and after (grey trace) exhaustive electrolysis at E_{app} = – 1.85 V ($2e^-$ passed, RDE in dashes lines). B) Cyclic voltammograms of [$\mathbf{1}^{IV}$] (1 mM in THF + TBA.TFSI (0.1 M)) recorded before (full black line) and after

addition of i) 1 molar equivalent of TBACl (full grey line: [$\mathbf{9}^{IV}$]) and ii) TBACl in excess (dashed black line: [$\mathbf{10}^{IV}$]$^{-}$). Scan rate: 100 mV.s^{-1} (20 mV.s^{-1} for RDE measurement at 500 rpm). Working electrode: GC (∅ 3 mm), counter electrode: Pt, reference: Ag^{+}(10^{-2} M)/Ag. Electrolysis on glassy carbon foam at – 1.85 V (2 e^{-} per molecules), counter electrode: carbon in DMF TBA.TFSI │ THF TBA.TFSI.

As can be seen in Figure 6B, the addition of one equivalent of tetra-*n*-butylammonium chloride to a THF solution of [$\mathbf{1}^{IV}$] led to a large cathodic shift (ΔE_p = – 250 mV) of the initial oxidation wave coming along with a loss of reversibility (Figure 6B, grey solid line). Consistent with the known lability of the Mo-I bond, this irreversible wave was attributed to the oxidation of the chloride complex [$\mathbf{9}^{IV}$] [($P^{Ph}P_2^{Cy}$)Mo(≡N)(Cl)] obtained after substitution of iodide by chloride on the Mo^{IV} center. The presence of free iodide was confirmed by the observation of an intense irreversible oxidation wave at E_p = 0 V. Further studies revealed that [$\mathbf{9}^{IV}$] slowly evolves after addition of an excess TBACl towards the bis chloride complex [$\mathbf{10}^{IV}$]$^{-}$ ([($P^{Ph}P_2^{Cy}$)Mo(≡N)($Cl)_2$]$^{-}$). This conversion led to the disappearance of the initial oxidation wave at E_p = – 0.92 V (grey solid line in Figure 6B) in favor of a new irreversible wave emerging at E_p = – 0.7 V (black dashed line in Figure 6B) attributed to the one electron oxidation of [$\mathbf{9}^{IV}$]$^{-}$. The similarities observed between the signatures recorded after exhaustive reduction of [$\mathbf{2}^{III}$] [($P^{Ph}P_2^{Cy}$)$Mo^{III}Cl_3$] in the presence of N_2 (grey solid line in Figure 6A) and after addition of an excess chloride on [$\mathbf{1}^{IV}$] (black dashed line in Figure 6B) led us to conclude that the same anionic nitrido complex [$\mathbf{10}^{IV}$]$^{-}$ is formed in both conditions.

The involvement of [$\mathbf{2}^{III}$] [($P^{Ph}P_2^{Cy}$)$MoCl_3$] in the catalytic process and its ability to promote the reduction of nitrogen in presence of Cy_2BCl was eventually demonstrated with electrochemical studies carried out with [$\mathbf{2}^{III}$] under catalytic conditions. We first found that cyclic voltammograms of [$\mathbf{2}^{III}$] (1 mM in THF/TBATFSI) recorded after addition of 30 equivalents of Cy_2BCl and 1.5 equivalent of TBA.I display an intense "catalytic" reduction wave at E_p = – 2.26 V (Figure S13), similar to that observed in similar conditions with the nitride complex [$\mathbf{1}^{IV}$] (see Figure 3). The catalytic nature of the later wave, and the

ability of [$\mathbf{2}^{III}$] to convert N_2 in (boryl)amine, was then confirmed with controlled potential electrolysis performed in these conditions under N_2 at E_{app} = – 2.7 V yielding 2.3 ± 0.2 equivalents of NH_4^+ (yield = 23 ± 2 %, Faradaic efficiency = 23 ± 1 %, average of two experiments).

All the experimental data discussed above are thus consistent with the mechanism shown in Scheme 3. The first step is a fast addition of Cy_2BCl on [$\mathbf{1}^{IV}$] [($P^{Ph}P_2^{Cy}$)Mo(≡N)(I)] yielding the imido complex [$\mathbf{4}^{IV}$] [($P^{Ph}P_2^{Cy}$)Mo^{IV}(=NBCy_2)(I)(Cl)]. Under electrochemical conditions, *i.e.* in presence of large amounts of supporting electrolyte, the iodide ligand is readily displaced by solvent molecule to form complex [$\mathbf{3}^{IV}$]$^+$. Stoichiometric reactions coupled to DFT computations demonstrate the unfavorable addition of a second Cy_2BCl molecule to afford the bis-borylamido complex. On the other hand, in situ generation of "HX" from mixtures of Cy_2BCl/TBA.TFSI and I^- provides a low energy pathway to [$\mathbf{5}^{IV}$]$^+$ [($P^{Ph}P_2^{Cy}$)Mo^{IV}(NHBCy_2)Cl_2]$^+$. The reduced nucleophilic character of the amido cationic complex [$\mathbf{5}^{IV}$]$^+$ requires a reduction of the metallic center to allow subsequent functionalization. The latter complex can be reduced at E = – 0.85 V to afford [$\mathbf{5}^{III}$] which is readily converted in [$\mathbf{2}^{III}$] and NH(BCy_2)$_2$ in the presence of Cy_2BCl. Then, closing the cycle, a two-electron reduction of [$\mathbf{2}^{III}$] in the presence of N_2 affords back the chloride analogue [$\mathbf{9}^{IV}$] [($P^{Ph}P_2^{Cy}$)Mo(≡N)(Cl)] of the initial complex [$\mathbf{1}^{IV}$].

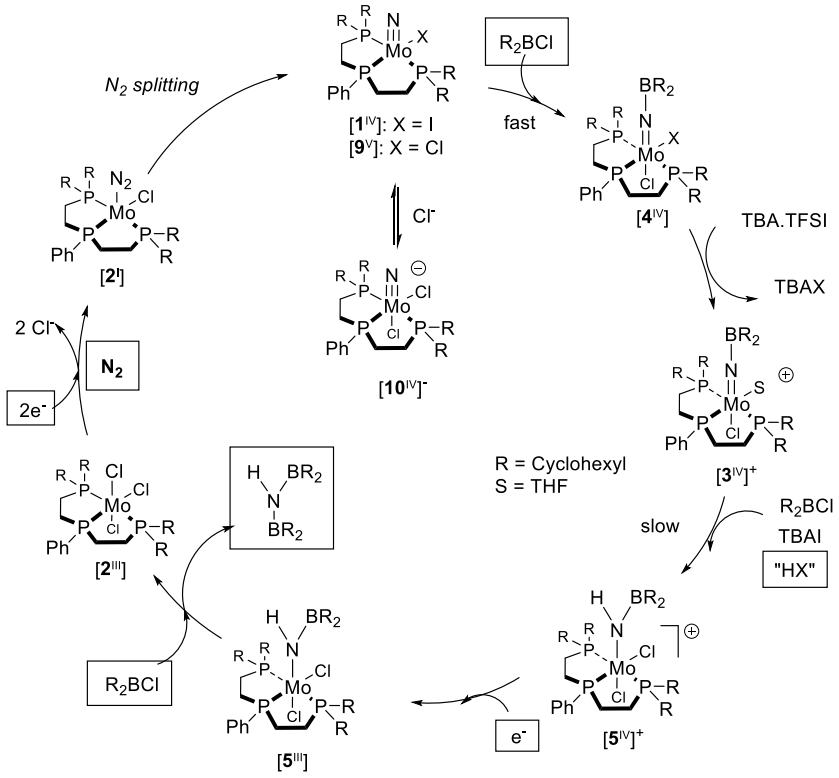

Scheme 3. Proposed mechanism for the electrocatalytic reduction of N_2 based on electrochemical/chemical/theoretical coupled investigations.

Conclusion

In conclusion, we reported here the first electrocatalytic reduction of nitrogen to aminoboranes with Faradaic yield up to 38%, challenging the most efficient homogeneous-phase electrocatalytic processes reported so far.[2,28] By coupling electrochemical and spectroscopic techniques, we were able to understand the behavior of the Mo^{IV} complex in the presence of Cy_2BCl and showed the essential role of the solvent and the electrolyte on the reactivity of the Mo≡N triple bond and on the exchanges of ligands on the metal center.

These in-depth analyzes also allowed us to propose a catalytic cycle and to identify several key species involved in this transformation including the unexpected (boryl)amido complex $[\mathbf{5}^{IV}]^+$ $[(P^{Ph}P_2{}^{Cy})Mo^{IV}(NHBCy_2)Cl_2]^+$, formed only in electrolytic conditions, and the trischloride Mo^{III} complex $[\mathbf{2}^{III}]$ $[(P^{Ph}P_2{}^{cy})MoCl_3]$, whose ability to split N_2 under application of a suitable electrochemical potential was demonstrated. Our study highlights the favorable generation of acid source in the reaction medium,

providing a lower energy pathway for N functionalization. Efforts are currently focused taking advantage of this understanding to improve the electrocatalytic efficiency of this process as well as on extending this strategy to other electrophiles.

EXPERIMENTAL SECTION

General considerations. THF (anhydrous, ≥ 99.9 %, inhibitor free) used for our studies was purchased from Sigma-Aldrich and purified over activated alumina before use. DMF (anhydrous, ≥ 99,9 %), HCl (2 M in Et_2O), and acetonitrile (anhydrous, ≥ 99,9 %) were purchased from Sigma-Aldrich and Thermo Fisher Scientific (AcroSeal™ and Sure/Seal™ packaging) and used as received. Tetra-n-butylammonium bis-trifluoromethanesulfonimidate was synthesized from tetrabutylammonium hydroxide (40 % weight solution in water, Sigma-Aldrich) and lithium bis-trifluoromethanesulfonimidate (99.95 %, Sigma-Aldrich), recrystallized several times in EtOH (absolute)/H_2O then dried at 50-60 °C under vacuum before use. The nitrido complex [$\mathbf{1}^{IV}$] and the trichloro complex [$\mathbf{2}^{III}$] have been synthesized following known procedures.[6,8,26] . Cy_2BCl (1 M in hexane) and HCl (1 M in Et_2O) were obtained from Sigma-Aldrich and used without further purification (Sure/Seal™ packaging). TBA.Cl and TBA.I were obtained from Sigma-Aldrich and dried under vacuum during 2-3 days at 50 °C before use. DMSO-d_6 was purchased from Euristop and used as received. Deuterated solvents were purchased from Euristop, stored on molecular sieves and degased by freeze-pump-thaw method. Triethylamine was purchased from Sigma-Aldrich, distillated over NaOH, stored on molecular sieves and degased by freeze-pump-thaw method. Electrochemical measurements were carried out using a Biologic SP-300 potentiostat equipped with a ±1A/±48 V booster. All studies were conducted inside a glovebox, under a nitrogen atmosphere, in home-made one-compartment, three-electrode electrochemical cells. An automatic ohmic drop compensation procedure was systematically implemented when using cyclic voltammetry. Cyclic voltammetry measurements were recorded at a vitreous carbon electrode (Ø = 3 mm, ALS instruments). Voltamperometry measurements at rotating disk electrodes (RDE) were carried out with a radiometer

(CTV101 radiometer analytical) equipment at a rotation rate of 500 rpm using a glassy carbon RDE tip (Ø= 3 mm). Working electrodes were systematically polished before use with diamond paste (average diameter of particles: 2 µm, PRESI SA). All measurements (analytic and electrolysis) were conducted using a reference electrode made of a silver wire dipped in a solution of silver nitrate (10^{-2} M $Ag(NO_3)$ in CH_3CN $TBAPF_6$ 0,1 M). A glass guard filled with electrolyte was used to avoid leaks of silver ions inside the electrolytic solution. The counter electrode used for all analytical studies was a Pt wire. Electrolysis were conducted in a home-made divided cell using freshly cut carbon foam (vitreous carbon foam 3000C VC003837 obtained from Goodfellow) average dimensions: 1 cm x 1 cm) as a working electrode connected by a rod of glassy carbon. The counter electrode was a rod of graphite. A magnetic bar was introduced to stir the solution during electrolysis. Spectroscopic measurements were conducted using a UV-NIR Zeiss MCS-601 spectrophotometer using a quartz immersion probe (Hellma, optical path 1 mm), or with quartz cuvettes (Hellma, optical path 1 cm or MB-Thuet, optical path 5 or 1 mm). ^{1}H,^{31}P, ^{11}B and ^{13}C NMR data were collected on a Bruker Advance 300 MHz (121.5 MHz for ^{31}P), 500 MHz (160.42 MHz for ^{11}B) or 600 MHz (150.9 MHz for ^{13}C) using valved NMR tubes purchased from Norell. ^{11}B NMR spectra were recorded using an ECHOIG sequence.[38] ESR spectra were collected at 110K using a Bruker E500 spectrometer operated at a single frequency X-Band (9.4 GHz) and a rectangular cavity (ST520) with 100 KHz modulation frequency. The instrument settings were as follows: microwave power: 22mW; modulation amplitude: 1 G; Hyperfine coupling constants a and g values were obtained with a simulation of experimental spectra using easyspin (Matlab toolbox).[39]

Typical procedure for cyclic voltammetry measurement. Inside a N_2-regulated glove box, a freshly prepared solution of TBA.TFSI (0,1 M, 106 mg) in 2 mL of dry THF was introduced inside a four necks, one compartment electrochemical cell containing a polished working electrode (vitreous carbon, Ø: 3 mm), a platinum wire counter electrode and a Ag^{+}/Ag reference electrode (separated from the solution by a glass guard filled with a THF/TBA.TFSI solution). The purity of the electrolyte was first checked by conducting CV measurements over the accessible potential range (– 3.2 V and + 1.4 V). The species

under study was added as a solid to reach a 1 mM concentration. The working electrode was systematically polished/washed with THF between all measurements. The reference electrode was calibrated at the end of all studies using ferrocene as an internal standard.

Typical procedure for electrolysis. All manipulations were conducted inside a N_2-regulated glove box. Control potential electrolysis were conducted in a home-made one compartment cell containing 2 mL of a 0.1 M solution of TBATFSI (105 mg) in THF, 1.6 mg of catalyst (1 mM) and a given volume of Cy_2BCl in hexane (1 M). Cyclic voltammograms (CV) were systematically recorded before and after addition of the reactants over the accessible potential range (– 3.2 V to + 1.4 V) to check the purity of the samples. A piece of vitreous carbon foam (1 x 1 cm) was used as working electrode and a large piece of graphite placed in a guard filled with a solution of DMF + TBATFSI (0.1 M) was used as a counter electrode. A magnetic bar was introduced to stir the mixture. Electrolysis were conducted in potentiostatic regime, which involved setting the potential of the working electrode and recording the charge during the whole experiment. The electrolysis was stopped after reaching a given charge or when the measured current became negligible (stabilized charge or current < 6 % of its initial value). The advancement of the reaction was followed by conducting RDE and CV measurements on the electrolyzed solution. NMR was used to quantify the amount of ammonium formed at the end of a given experiment using a well-established protocol.[38] This was achieved upon transferring 0.5 mL of the electrolyzed solution in a valved NMR tube which was sealed and taken outside the glovebox. Hydrolysis of borylamine was then achieved by addition of 0.1 mL of HCl in Et_2O (2 M). The NMR tube was then connected to a vacuum line to remove all volatile compounds and afford a white solid. The residue was then solubilized in DMSO-d_6 in the presence of 1,3,5-trimethoxybenzene as an internal standard. The amount of ammonium formed was thus quantified by NMR measurement *via* integration of the multiplet centered at 7.2 ppm (t, $^1J(N\text{-}H) = 51$ Hz) *vs*. trimethoxybenzene. As the quantity of ammonium obtained is directly linked to the quantity of aminoboranes obtained after electrolysis, the yield is obtained by the formula $3n(NH_4^+)/n(Cy_2BCl)$, where $n(NH_4^+)$ is quantity of ammonium assessed by NMR and $n(Cy_2BCl)$ is the

number of moles of chloroborane introduced in the cell before electrolysis. The TON is calculated by the formula $n(NH_4^+)/n(\mathbf{1})$, where n(**1**) is the quantity of catalyst added before electrolysis. The Faradaic yield was calculated using the formula $3n(NH_4^+)F/Q$ where $n(NH_4^+)$ is quantity of ammonium assessed by NMR, F the Faradaic constant and Q the total charge passed during controlled potential electrolysis.

For manipulations under argon, the cell was first prepared in an Ar-filled glovebox with the same elements and reactants described above (THF was degassed and saturated with argon by freeze-pump-thawn method). The cell is then sealed and the electrolysis was performed outside the glovebox. The treatment of the aliquot and the quantification of the ammonium produced was done as above.

For the controlled potential electrolysis of [$\mathbf{1}^{IV}$] + 5 equivalents of HCl, in the absence of Cy_2BCl, the same cell is filled with a 8 mL THF TBA.TFSI (0.1 M, 418 mg). Then [$\mathbf{1}^{IV}$] (1 mM, 6.4 mg) and HCl (1 M in diethylether, 40 µL) are added in the cell. The electrodes used remain the same than above. The potential is the set at – 2.7 V (*vs*. Ag^+/Ag) and the electrolysis is run until – 3.2 C is passed. The quantification of the ammonia produced was done as above.

Hydrolysis of [$\mathbf{1}^{IV}$] and ammonia quantification. Inside a N_2-regulated glove box, 7.5 mg (9.4 µmol) of [$\mathbf{1}^{IV}$] was dissolved in 0.5 mL of THF and the solution obtained was transferred in a J-Young NMR tube. 0.1 mL of an HCl solution (1 M in Et_2O) is then added and the solvent is evaporated under vacuum. The residual solid is then dissolved in 0.5 mL dmso-d6 and 3.1 mg 1,3,5-trimethoxybenzene is added as an internal standard. The amount of ammonium formed was then quantified by NMR measurement *via* integration of the multiplet centered at 7.2 ppm (t, $^1J(N-H)$ = 51 Hz) *vs*. trimethoxybenzene

In situ synthesis of [$\mathbf{5}^{IV}$]$^+$. Method A) Using Cy_2BCl then HCl: Inside a N_2-regulated glove box, 2.4 mg (3 µmol) of [$\mathbf{1}^{IV}$] was dissolved in 3 mL THF TBA.TFSI (0.1 M, 156.8 mg). 3 µL of a solution of Cy_2BCl 1 M in hexane (3 µmol) is then added to the mixture and the solution turned from brown to green, characteristic of the in situ formation of [$\mathbf{4}^{IV}$] (Figure S15). Then a quantity of HCl (1 M in Et_2O) ranging

from 6 µL to 15 µL (6 µmol to 15 µmol) was added on in situ formed $[\mathbf{5}^{\mathbf{IV}}]^+$ resulting in color change from green to yellow. The in situ formed $[\mathbf{5}^{\mathbf{IV}}]^+$ was then characterized by cyclic voltammetry.

Method B) Using Cy_2BCl only: Inside a N_2-regulated glove box, 2.4 mg (3 µmol) of $[\mathbf{1}^{IV}]$ was dissolved in 3 mL THF TBA.TFSI (0.1 M, 156.8 mg). A quantity of Cy_2BCl 1 M in hexane ranging from 6 µL to 15 µL (6 µmol to 15 µmol) is added on $[\mathbf{3}^{IV}]$ resulting in color change from brown to yellow. The in situ formed $[\mathbf{5}^{\mathbf{IV}}]^+$ was then characterized by cyclic voltammetry.

Method C) Using TlTFSI: Inside a N_2-regulated glove box, 7,4 mg of $[\mathbf{1}^{IV}]$ (9.3 µmol) was dissolved in 0.5 mL of THF-d_8. Then, 9.3 µL of Cy_2BCl 1 M in hexane (9.3 µmol, 1 equivalent) was added to the mixture. 4.5 mg of TlTFSI (9.3 µmol) is then added to the mixture, which lead to the instantaneous precipitation of TlI. The mixture is then filtered and 9.3 µL of HCl 1 M in diethylether (9.3 µmol) is added to the mixture. The tube is then analyzed by NMR and by cyclic voltammetry, and the spectra with the corresponding voltammograms could be found in the supplementary informations.

Reactions of Cy_2BCl and TBAI in THF: evidence of acid generation. Cy_2BCl + TBAI (5:1) in THF*:* Inside a N_2-regulated glove box, 3.7 mg of TBAI (10 µmol*)* was dissolved in 10 mL THF. Then 50 µL of Cy_2BCl 1 M in hexane (*50* µmol, 5 equivalents) was added and the mixture was stirred overnight. An aliquot of 0.6 mL was put in a J-Young NMR tube, C_6D_6 was added and a ^{11}B NMR spectrum was acquired (ECHOIG, 160.42 MHz). For ^1H, ^{13}C, ^1H-^1H COSY, ^1H-^{13}C HSQC and ^1H-^{13}C HMBC spectrum, a 0.6 mL aliquot is put in a J-Young NMR tube, and the solvent was evaporated under vacuum. The solid residue was then dissolved in C_6D_6. The spectra are found Figure S18-S23.The interpretation of the spectra leads to the partial identification of two products coming from the THF ring opening reaction with Cy_2BCl (see SI). In the region below 2 ppm are found signals of Cy moieties and *N*-tetrabutylammonium.$^{11}B\{^1H\}$ NMR (ECHOIG, D20 = 250 µs, 160.42 MHz, THF/C_6D_6, 25°C, Figure S18), δ: 15.6 ppm (Cy_2BH), 23.2 ppm ($Cy_2BCl.THF$), 30.7 ppm ($(Cy_2BH)_2$), 51.2 ppm (Cy_2B-OR). ^1H NMR **(**600 MHz, Figure S19, see SI for the attribution and the identification of THF ring opening products) and ^{13}C NMR spectrum (150.9 MHz, Figure S20, see SI for the attribution and the identification

of THF ring opening products) allowed the identification of two related compounds resulting from THF ring opening and attack by I^- and Cl^- (identified by comparison to their known spectra, see SI). Several other coupled signals in the 3-4 ppm region point to other products resulting from THF opening. Cy_2BCl + TBAI (1:1) in THF*:* in order to demonstrate the formation of acid in the Cy_2BCl / I^- / THF mixtures, proton trapping with triethylamine was realized**:** inside a *N*2-regulated glove box, 111 mg of TBAI (300 µmol) was dissolved in 10 mL of THF. Then 300 µL of Cy_2BCl 1 M in hexane (300 µmol, 1 equivalent) was added and the mixture was stirred overnight. The evolution of the reaction could be followed by the progressive dissolution of the TBAI in THF. 40 µL of previously dried and distilled triethylamine (300 µmol) was added to the mixture, resulting in the immediate formation of a white precipitate. The precipitate was filtrated, washed 3 times with 5 mL THF and dried under vacuum. The presence of Et_3NH^+ was confirmed by ^1H NMR (Figure S24) by the signals at δ: 1.26-1.31 ppm (t, 9H, CH_3), 2.98-3.07 ppm (m, 6H, CH_2), 11.69 ppm (s, 1H, NH); NBu_4^+ signals are present on the spectrum: δ: 0.9 ppm (t, 9H, CH_3), 1.3 ppm (m, 8H, CH_2), 1.6 ppm (m, 6H, CH_2), 3.1 ppm (m, 6H, C*H*2-N, mixed with the 6H of Et_3NH^+).

DFT calculations. Geometry optimizations were performed using Gaussian 16 (Revision C01)[41] at the PBE0 level of hybrid density functional theory,[42] with inclusion of D3(bj) corrections in the optimization process.[43,44] The geometries of all located extrema are given as xyz coordinates data in a separate file (Geom.xyz) in the SI. The atoms H, B, C, N, P, O, F, S, and Cl were represented by an svp basis set.[45] The Mo and I atoms were represented by Dolg's pseudo potential and the associated basis set.[46,47] The solvent (THF) influence was taken into consideration through single-point calculations on the gas-phase optimized geometries with SCRF calculations within the SMD model.[48] For the SCRF calculations, the atoms were treated with a def2-qzvp basis set.[49] All energies reported are Gibbs free energies obtained at 298 K and 1atm using a procedure described by Ariai and Gellrich in a recent paper to better described the entropy penalty for associative reactions.[50] The procedure described by equation 14 in reference 50 has been considered : E_{elst} is obtained in single point calculations with implicit inclusion of the solvent

(THF) by substracting the non-electrostatic component from the converged energy. The entropy contribution of each species is computed from the frequency calculations output using a script obtained from the authors of reference 50.

AUTHOR INFORMATION

Corresponding Authors

***Nicolas Mézailles** – Laboratoire Hétérochimie Fondamentale et appliquée, Université Paul Sabatier, CNRS, 31062 Toulouse Cedex, France. Email: nicolas.mezailles1@univ-tlse3.fr

***Christophe Bucher** – CNRS, ENS de Lyon, LCH, UMR 5182, 69342, Lyon cedex 07, France. Email: christophe.bucher@ens-lyon.fr

Authors

Théo Personeni – ENS de Lyon, CNRS, LCH, UMR 5182, 69342, Lyon cedex 07, France / Laboratoire Hétérochimie Fondamentale et appliquée, Université Paul Sabatier, CNRS, 31062 Toulouse Cedex, France

Barbara Rialland – Laboratoire Hétérochimie Fondamentale et appliquée, Université Paul Sabatier, CNRS, 31062 Toulouse Cedex, France

Idir Benaissa – Laboratoire Hétérochimie Fondamentale et appliquée, Université Paul Sabatier, CNRS, 31062 Toulouse Cedex, France. Present address: Institute of Science, Technology and Innovation-UM6P, Hay Moulay Rachid, BP43150 Benguerir, Morocco

Soukaina Bennaamane – Laboratoire Hétérochimie Fondamentale et appliquée, Université Paul Sabatier, CNRS, 31062 Toulouse Cedex, France

Lhoussain Khrouz – ENS de Lyon, CNRS, LCH, UMR 5182, 69342, Lyon cedex 07, France

Andrea Mulas – ENS de Lyon, CNRS, LCH, UMR 5182, 69342, Lyon cedex 07, France

Marie Fustier-Boutignon – Laboratoire Hétérochimie Fondamentale et appliquée, Université Paul Sabatier, CNRS, 31062 Toulouse Cedex, France

Eric Clot – ICGM, Univ. Montpellier, CNRS, ENSCM, Montpellier, France

Present Addresses

† Institute of Science, Technology and Innovation-UM6P, Hay Moulay Rachid, BP43150 Benguerir, Morocco

Author Contributions

The manuscript was written through contributions of all authors. All authors have given approval to the final version of the manuscript.

Funding Sources

ANR (ANR-23-CE07-0049-02)

Ecole Normale Supérieure de Lyon (Projet emergence, PhD funding to TP)

Ecole Polytechnique (PhD funding for BR)

CALMIP (Grant 2021-P1310)

Supporting informations: Additional experimental details, materials and methods including supplementary cyclic voltammograms, UV-visible, EPR and NMR spectra.

ACKNOWLEDGMENT

Financial support from CNRS, ANR (ANR-23-CE07-0049-02) and from the Ecole Normale Supérieure de Lyon (Projet emergence, PhD funding to TP) and the Ecole Polytechnique (PhD funding for BR) is acknowledged. This work was performed using HPC resources from CALMIP (Grant 2021-P1310). The NMR service of the ICT (UAR 2599) is acknowledged.

ABBREVIATIONS

CE: counter electrode, Cy: cyclohexyl, DMF: dimethylformamide, Et: ethyl, GC: glassy carbon, RDE: rotating disk electrode, TBA.TFSI: tetra-*n*-butylammonium bis-trifluoromethanesulfonimidate, THF: tetrahydrofuran, WE: working electrode

REFERENCES

(1) Walter, M. D. Recent Advances in Transition Metal-Catalyzed Dinitrogen Activation. In *Advances in Organometallic Chemistry*; Elsevier Inc., 2016; Vol. 65, pp 261–377.

(2) Chalkley, M. J.; Drover, M. W.; Peters, J. C. Catalytic N_2 -to-NH_3 (or -N_2H_4) Conversion by Well-Defined Molecular Coordination Complexes. *Chem. Rev.* **2020**, *120*, 5582–5636.

(3) Roux, Y.; Duboc, C.; Gennari, M. Molecular Catalysts for N_2 Reduction: State of the Art, Mechanism, and Challenges. *ChemPhysChem* **2017**, *18*, 2606–2617.

(4) Shipman, M. A.; Symes, M. D. Recent Progress towards the Electrosynthesis of Ammonia from Sustainable Resources. *Catal. Today* **2017**, *286*, 57–68.

(5) Ashida, Y.; Arashiba, K.; Nakajima, K.; Nishibayashi, Y. Molybdenum-Catalysed Ammonia Production with Samarium Diiodide and Alcohols or Water. *Nature* **2019**, *568*, 536–540.

(6) Bennaamane, S.; Espada, M. F.; Mulas, A.; Personeni, T.; Saffon-Merceron, N.; Fustier-Boutignon, M.; Bucher, C.; Mézailles, N. Catalytic Reduction of N_2 to Borylamine at a Molybdenum Complex. *Angew. Chem. Int. Ed.* **2021**, *60*, 20210–20214.

(7) Tanabe, Y.; Nishibayashi, Y. Recent Advances in Catalytic Nitrogen Fixation Using Transition Metal–Dinitrogen Complexes under Mild Reaction Conditions. *Coord. Chem. Rev.* **2022**, *472*, 214783.

(8) Liao, Q.; Saffon-Merceron, N.; Mézailles, N. N_2 Reduction into Silylamine at Tridentate Phosphine/Mo Center: Catalysis and Mechanistic Study. *ACS Catal.* **2015**, *5*, 6902–6906.

(9) Yandulov, D. V.; Schrock, R. R. Catalytic Reduction of Dinitrogen to Ammonia at a Single Molybdenum Center. *Science* **2003**, *301*, 76–78..

(10) Komori, K.; Oshita, H.; Mizobe, Y.; Hidai, M. Preparation and Properties of Molybdenum and Tungsten Dinitrogen Complexes. 25. Catalytic Conversion of Molecular Nitrogen into Silylamines Using Molybdenum and Tungsten Dinitrogen Complexes. *J. Am. Chem. Soc.* **1989**, *111*, 1939–1940.

(11) Forrest, S. J. K.; Schluschaß, B.; Yuzik-Klimova, E. Y.; Schneider, S. Nitrogen Fixation via Splitting into Nitrido Complexes. *Chem. Rev.* **2021**, *121*, 6522–6587.

(12) Mézailles, N. 1.22 - Reactivity and Structure of Complexes of Small Molecules: Dinitrogen. In *Comprehensive Coordination Chemistry III*; Constable, E. C., Parkin, G., Que Jr, L., Eds.; Elsevier: Oxford, 2021; pp 875–958.

(13) Kim, S.; Loose, F.; Chirik, P. J. Beyond Ammonia: Nitrogen–Element Bond Forming Reactions with Coordinated Dinitrogen. *Chem. Rev.* **2020**, *120*, 5637–5681.

(14) Tanaka, H.; Sasada, A.; Kouno, T.; Yuki, M.; Miyake, Y.; Nakanishi, H.; Nishibayashi, Y.; Yoshizawa, K. Molybdenum-Catalyzed Transformation of Molecular Dinitrogen into Silylamine: Experimental and DFT Study on the Remarkable Role of Ferrocenyldiphosphine Ligands. *J. Am. Chem. Soc.* **2011**, *133*, 3498–3506.

(15) Ashida, Y.; Mizushima, T.; Arashiba, K.; Egi, A.; Tanaka, H.; Yoshizawa, K.; Nishibayashi, Y. Catalytic Production of Ammonia from Dinitrogen Employing Molybdenum Complexes Bearing N-Heterocyclic Carbene- Based PCP-Type Pincer Ligands. *Nat. Synth* **2023**, *2*, 635–644.

(16) Lindley, B. M.; Appel, A. M.; Krogh-Jespersen, K.; Mayer, J. M.; Miller, A. J. M. Evaluating the Thermodynamics of Electrocatalytic N_2 Reduction in Acetonitrile. *ACS Energy Lett.* **2016**, *1* (4), 698–704.

(17) Sherbow, T. J.; Thompson, E. J.; Arnold, A.; Sayler, R. I.; Britt, R. D.; Berben, L. A. Electrochemical Reduction of N_2 to NH_3 at Low Potential by a Molecular Aluminum Complex. *Chem. – Eur. J.* **2019**, *25*, 454–458.

(18) Zhuo, Q.; Yang, J.; Mo, Z.; Zhou, X.; Shima, T.; Luo, Y.; Hou, Z. Dinitrogen Cleavage and Functionalization with Carbon Dioxide in a Dititanium Dihydride Framework. *J. Am. Chem. Soc.* **2022**, *144*, 6972–6980.

(19) Merakeb, L.; Robert, M. Advances in Molecular Electrochemical Activation of Dinitrogen. *Curr. Opin. Electrochem.* **2021**, *29*, 100834.

(20) Alten, R. S.; Wätjen, F.; Demeshko, S.; Miller, A. J. M.; Würtele, C.; Siewert, I.; Schneider, S. (Electro-)Chemical Splitting of Dinitrogen with a Rhenium Pincer Complex. *Eur. J. Inorg. Chem.* **2020**, *2020*, 1402–1410.

(21) Lindley, B. M.; van Alten, R. S.; Finger, M.; Schendzielorz, F.; Würtele, C.; Miller, A. J. M.; Siewert, I.; Schneider, S. Mechanism of Chemical and Electrochemical N_2 Splitting by a Rhenium Pincer Complex. *J. Am. Chem. Soc.* **2018**, *140*, 7922–7935.

(22) Munisamy, T.; Schrock, R. R. An Electrochemical Investigation of Intermediates and Processes Involved in the Catalyticreduction of Dinitrogen by [HIPTN3N]Mo (HIPTN3N = (3,5-(2,4,6-i-Pr3C6H2)2C6H3NCH2CH2)3N). *Dalton Trans* **2012**, *41*, 130–137.

(23) Bruch, Q. J.; Malakar, S.; Goldman, A. S.; Miller, A. J. M. Mechanisms of Electrochemical N_2 Splitting by a Molybdenum Pincer Complex. *Inorg. Chem.* **2022**, *61*, 2307–2318.

(24) Pickett, C. J.; Talarmin, J. Electrosynthesis of Ammonia. *Nature* **1985**, *317*, 652–653.

(25) Katayama, A.; Ohta, T.; Wasada-Tsutsui, Y.; Inomata, T.; Ozawa, T.; Ogura, T.; Masuda, H. Dinitrogen-Molybdenum Complex Induces Dinitrogen Cleavage by One-Electron Oxidation. *Angew. Chem. Int. Ed.* **2019**, *58*, 11279–11284.

(26) Espada, M. F.; Bennaamane, S.; Liao, Q.; Saffon-Merceron, N.; Massou, S.; Clot, E.; Nebra, N.; Fustier-Boutignon, M.; Mézailles, N. Room-Temperature Functionalization of N_2 to Borylamine at a Molybdenum Complex. *Angew. Chem. Int. Ed.* **2018**, *57*, 12865–12868.

(27) Chalkley, M. J.; Del Castillo, T. J.; Matson, B. D.; Peters, J. C. Fe-Mediated Nitrogen Fixation with a Metallocene Mediator: Exploring p K_a Effects and Demonstrating Electrocatalysis. *J. Am. Chem. Soc.* **2018**, *140*, 6122–6129.

(28) Garrido-Barros, P.; Derosa, J.; Chalkley, M. J.; Peters, J. C. Tandem Electrocatalytic N2 Fixation via Proton-Coupled Electron Transfer. *Nature* **2022**, *609*, 71–76.

(29) Ibrahim, A. F.; Garrido-Barros, P.; Peters, J. C. Electrocatalytic Nitrogen Reduction on a Molybdenum Complex Bearing a PNP Pincer Ligand. *ACS Catal.* **2023**, 72–78.

(30) Chalkley, M. J.; Garrido-Barros, P.; Peters, J. C. A Molecular Mediator for Reductive Concerted Proton-Electron Transfers via Electrocatalysis. *Science* **2020**, *369*, 850–854.

(31) Arashiba, K.; Miyake, Y.; Nishibayashi, Y. A Molybdenum Complex Bearing PNP-Type Pincer Ligands Leads to the Catalytic Reduction of Dinitrogen into Ammonia. *Nat. Chem.* **2011**, *3*, 120–125.

(32) Bennaamane, S.; Rialland, B.; Khrouz, L.; Fustier-Boutignon, M.; Bucher, C.; Clot, E.; Mézailles, N. Ammonia Synthesis at Room Temperature and Atmospheric Pressure from N_2 : A Boron-Radical Approach. *Angew. Chem. Int. Ed.* **2023**, *62*, e202209102.

(33) Bennaamane, S.; Espada, M. F.; Yagoub, I.; Saffon-Merceron, N.; Nebra, N.; Fustier-Boutignon, M.; Clot, E.; Mézailles, N. Stepwise Functionalization of N_2 at Mo: Nitrido to Imido to Amido – Factors Favoring Amine Elimination from the Amido Complex. *Eur. J. Inorg. Chem.* **2020**, *2020* , 1499–1505.

(34) Haufe, L. C.; Arrowsmith, M.; Dietz, M.; Gärtner, A.; Bertermann, R.; Braunschweig, H. Spontaneous N_2 -Diboranylation of $[W(N_2)_2(Dppe)_2]$ with $B_2Br_4(SMe_2)_2$. *Dalton Trans.* **2022**, *51*, 12786–12790.

(35) Ramachandran, P. V.; Zou, M.-F.; Brown, H. C. Efficient Synthesis of B-Iododialkyl- and B-Alkyldiiodoboranes as Their Acetonitrile Complexes: Application for the Enolboration–Aldolization of Ethyl Ketones. *Helv. Chim. Acta* **2002**, *85*, 3027–3032.

(36) Duman, L. M.; Sita, L. R. Closing the Loop on Transition-Metal-Mediated Nitrogen Fixation: Chemoselective Production of $HN(SiMe_3)_2$ from N_2 , Me_3SiCl, and X—OH (X = R, R_3Si, or Silica Gel). *J. Am. Chem. Soc.* **2017**, *139*, 17241–17244.

(37) Liao, Q.; Cavaillé, A.; Saffon-Merceron, N.; Mézailles, N. Direct Synthesis of Silylamine from N_2 and a Silane: Mediated by a Tridentate Phosphine Molybdenum Fragment. *Angew Chem Int Ed* **2016**, 5.

(38) Merakeb, L.; Bennaamane, S.; De Freitas, J.; Clot, E.; Mézailles, N.; Robert, M. Molecular Electrochemical Reductive Splitting of Dinitrogen with a Molybdenum Complex. *Angew. Chem.* **2022**, *61*, e202209899.

(39) Macho, J. M.; Blue, R. M.; Lee, H.-W.; MacMillan, J. B. Boron NMR as a Method to Screen Natural Product Libraries for B-Containing Compounds. *Org. Lett.* **2022**, *24*, 3161–3166.

(40) Stoll, S.; Schweiger, A. EasySpin, a Comprehensive Software Package for Spectral Simulation and Analysis in EPR. *J. Magn. Reson.* **2006**, *178*, 42–55.

(41) Frisch, M. J.; Trucks, G. W.; Schlegel, H. B.; Scuseria, G. E.; Robb, M. A.; Cheeseman, J. R.; Scalmani, G.; Barone, V.; Petersson, G. A.; Nakatsuji, H.; Li, X.; Caricato, M.; Marenich, A. V.; Bloino, J.; Janesko, B. G.; Gomperts, R.; Mennucci, B.; Hratchian, H. P.; Ortiz, J. V.; Izmaylov, A. F.; Sonnenberg, J. L.; Williams; Ding, F.; Lipparini, F.; Egidi, F.; Goings, J.; Peng, B.; Petrone, A.; Henderson, T.; Ranasinghe, D.; Zakrzewski, V. G.; Gao, J.; Rega, N.; Zheng, G.; Liang, W.; Hada, M.; Ehara, M.; Toyota, K.; Fukuda, R.; Hasegawa, J.; Ishida, M.; Nakajima, T.; Honda, Y.; Kitao, O.; Nakai, H.; Vreven, T.; Throssell, K.; Montgomery Jr., J. A.; Peralta, J. E.; Ogliaro, F.; Bearpark, M. J.; Heyd, J.

J.; Brothers, E. N.; Kudin, K. N.; Staroverov, V. N.; Keith, T. A.; Kobayashi, R.; Normand, J.; Raghavachari, K.; Rendell, A. P.; Burant, J. C.; Iyengar, S. S.; Tomasi, J.; Cossi, M.; Millam, J. M.; Klene, M.; Adamo, C.; Cammi, R.; Ochterski, J. W.; Martin, R. L.; Morokuma, K.; Farkas, O.; Foresman, J. B.; Fox, D. J. Gaussian 16 Rev. C.01, 2016.

(42) Adamo, C.; Barone, V. Toward Reliable Density Functional Methods without Adjustable Parameters: The PBE0 Model. *J. Chem. Phys.* **1999**, *110*, 6158–6170..

(43) Grimme, S.; Antony, J.; Ehrlich, S.; Krieg, H. A Consistent and Accurate Ab Initio Parametrization of Density Functional Dispersion Correction (DFT-D) for the 94 Elements H-Pu. *J. Chem. Phys.* **2010**, *132*, 154104.

(44) Grimme, S.; Ehrlich, S.; Goerigk, L. Effect of the Damping Function in Dispersion Corrected Density Functional Theory. *J. Comput. Chem.* **2011**, *32*, 1456–1465.

(45) Schäfer, A.; Horn, H.; Ahlrichs, R. Fully Optimized Contracted Gaussian Basis Sets for Atoms Li to Kr. *J. Chem. Phys.* **1992**, *97*, 2571–2577. https://doi.org/10.1063/1.463096.

(46) Peterson, K. A.; Figgen, D.; Goll, E.; Stoll, H.; Dolg, M. Systematically Convergent Basis Sets with Relativistic Pseudopotentials. II. Small-Core Pseudopotentials and Correlation Consistent Basis Sets for the Post-d Group 16–18 Elements. *J. Chem. Phys.* **2003**, *119*, 11113–11123.

(47) Andrae, D.; Häußermann, U.; Dolg, M.; Stoll, H.; Preuß, H. Energy-Adjustedab Initio Pseudopotentials for the Second and Third Row Transition Elements. *Theor. Chim. Acta* **1990**, *77*, 123–141.

(48) Marenich, A. V.; Cramer, C. J.; Truhlar, D. G. Universal Solvation Model Based on Solute Electron Density and on a Continuum Model of the Solvent Defined by the Bulk Dielectric Constant and Atomic Surface Tensions. *J. Phys. Chem. B* **2009**, *113*, 6378–6396.

(49) Weigend, F.; Ahlrichs, R. Balanced Basis Sets of Split Valence, Triple Zeta Valence and Quadruple Zeta Valence Quality for H to Rn: Design and Assessment of Accuracy. *Phys. Chem. Chem. Phys.* **2005**, *7*, 3297–3305.

(50) Ariai, J.; Gellrich, U. The Entropic Penalty for Associative Reactions and Their Physical Treatment during Routine Computations. *Phys. Chem. Chem. Phys.* **2023**, *25*, 14005–14015.

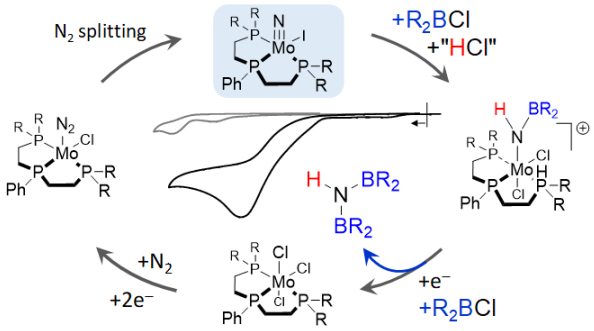

For table of content only